Water Science & Technology

IWA PUBLISHING

Water Science & Technology Vol 88 No 9, 2332 doi: 10.2166/wst.2023.292

Ion exchange synthesis of copper-based hydroxyapatite for the catalytic degradation of phenol

Yu Peng[a,b], Zhaobo Wang[a,b], Dajun Ren [a,b,*], Xiaoqing Zhang[a,b], Shuqin Zhang[a,b] and Wangsheng Chen[a,b]

[a] College of Resource and Environmental Engineering, Wuhan University of Science and Technology, Wuhan 430081, China
[b] Hubei Key Laboratory for Efficient Utilization and Agglomeration of Metallurgic Mineral Resources, Wuhan University of Science and Technology, Wuhan, Hubei 430081, China
*Corresponding author. E-mail: dj_ren@163.com

DR, 0000-0003-0752-4184

ABSTRACT

Hydroxyapatite (HAP) is a material renowned for its exceptional capabilities in adsorbing and exchanging heavy metal ions, making it a widely employed substance within the environmental domain. This study aims to present a novel material, namely copper–HAP (Cu–HAP), which was synthesized via an ion exchange method. The resulting material underwent comprehensive characterization using scanning electron microscopy, X-ray diffraction, Fourier-transform infrared spectroscopy, and Brunauer–Emmett–Teller (BET) analysis. Subsequently, based on the principle of the Fenton-like oxidation reaction, the material was used for the degradation of phenol. The outcomes of the investigation revealed that the optimal preparation conditions for the catalyst were achieved at a temperature of 40 °C, a pH value of 5, and a relative dosage of Cu–HAP at 100 mg/g. Under the reaction conditions of a catalyst dosage of 2 g/L, a 30% hydrogen peroxide concentration of 30 mM, a phenol concentration of 20 mg/L, a pH value of 6, a temperature of 40 °C, and the degradation rate of phenol impressively reached 98.12%. Furthermore, the degradation rate remained at 42.31% even after five consecutive cycles, indicating the promising potential of Cu–HAP in the treatment of recalcitrant organic compounds within this field.

Key words: catalyst, Fenton-like oxidation, hydroxyapatite, ion exchange, phenol, water treatment

HIGHLIGHTS

- A novel copper-based catalyst (Cu–HAP) has been synthesized and utilized for the catalytic degradation of phenol.
- Cu–HAP improved the efficiency of H_2O_2 in the traditional Fenton reaction.
- Cu–HAP surface has a rich pore structure.
- The phenol removal rate can still reach 42.31% after five times of reuse.

GRAPHICAL ABSTRACT

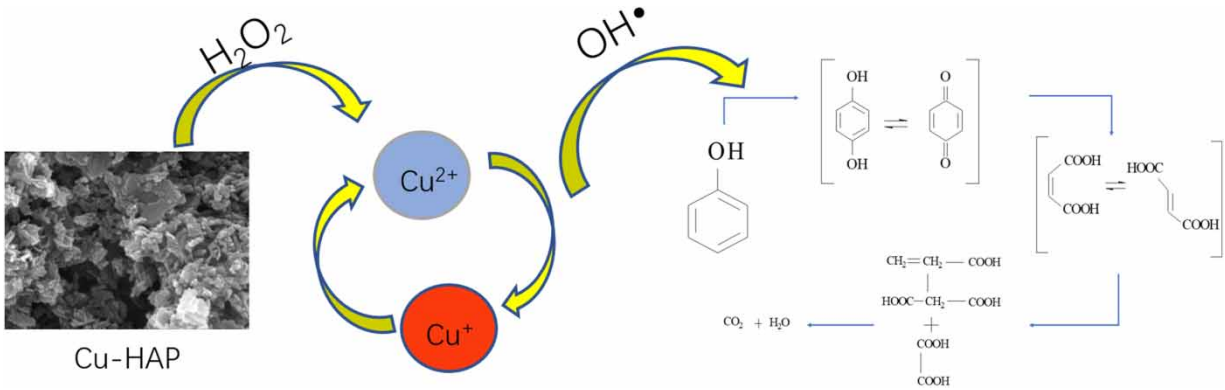

1. INTRODUCTION

Phenolic pollution primarily occurs in industrial wastewater, wherein phenolic compounds contribute to 40–80% of the total chemical oxygen demand (COD) in specific industrial effluents (Panigrahy *et al.* 2020). Due to their toxicity and carcinogenic properties, elevated concentrations of phenols in water can have detrimental effects on aquatic organisms and compromise liver and kidney functions upon human exposure. Consequently, it is imperative to treat industrial wastewater before its discharge into natural water bodies.

Presently, phenolic substance treatment methods primarily revolve around biological treatment (Qian *et al.* 2018; Jingxin *et al.* 2022), physical adsorption (Imane *et al.* 2023), chemical reduction, and chemical oxidation approaches. Among these, chemical oxidation methods hold immense potential as they can theoretically achieve the complete degradation of phenols, rendering them widely adopted. Notably, the advanced oxidation process (AOP) is recognized as a phenol chemical treatment technique with significant prospects for application (Santiago *et al.* 2002). An AOP surpasses the limitations of conventional oxidants, such as high cost and potential secondary environmental pollution. By generating highly reactive free radicals, including hydroxyl radicals ($HO^{\bullet}$) (Jian & Le 2012; Kuan & Huichun 2019), hydrogen peroxide radicals ($HO_2^{\bullet}$) (Weihua *et al.* 2022; Yu & Hefa 2022), superoxide radicals (O^{2-}) (Xiaoguang *et al.* 2018; Kuan & Huichun 2022), and singlet oxygen ($^1O_2$), recalcitrant organic pollutants can be effectively degraded and mineralized into low molecular weight products such as CO_2 and H_2O (Zhuangzhuang *et al.* 2023). Nevertheless, the traditional Fenton oxidation reaction heavily relies on operating conditions, such as medium pH, Fe^{2+} concentration, H_2O_2 content, reaction temperature, organic substance concentration, and the presence of other interfering agents in the solution. Notably, pH exerts a significant influence on the reaction process, as high pH values promote Fe^{2+} precipitation while facilitating H_2O_2 decomposition into O_2 and H_2O. Conversely, at pH values below 2.5, Fe^{2+} can form a complex $[Fe(H_2O)_6]^{2+}$, resulting in the sluggish generation of $HO^{\bullet}$ when reacting with H_2O_2, thereby severely impeding the reaction rate (Ramos *et al.* 2021).

Differing from the homogeneous Fenton system, the Fenton-like system incorporates metal ions such as Cr^{2+}, Ag^{+}, and Mg^{2+}, and certain organic pollutant degradation occurs under UV light conditions (Ludmila *et al.* 2020). In a hybrid system, organic molecules and H_2O_2 molecules are directly adsorbed onto the active sites on the catalyst surface, thereby enhancing the reaction efficiency. Moreover, catalyst recovery allows for pollutant treatment cost reduction and prevents catalyst-induced secondary pollution (Liu *et al.* 2019). Among them, the copper-based catalysts have excellent reactivity with H_2O_2 and a wide range of reaction pH, and the rate constant of Cu/Cu^{2+} for H_2O_2 is much higher than the advantage of the rate constant of Fe/Fe^{2+} (Lili *et al.* 2017).

Hydroxyapatite (HAP), with the chemical formula of $Ca_5(PO_4)_3(OH)$, widely exists in teeth, bones, and other materials. HAP has a high ion exchange capacity and good structural flexibility. OH^{-} in its structure can be replaced by F^{-}, Cl^{-}, and other anions, while Ca^{2+} can exchange with a variety of gold ions, such as Cd^{2+}, Pb^{2+}, Cu^{2+}, and Fe^{3+} (Zhaobo *et al.* 2022). A large number of experiments show that the performance of modified HAP can be significantly improved. Othmani *et al.* (2018) prepared Cu–HAP by coprecipitation, and the material showed good performance in the color change reaction of naphthol blue black solution where the reaction rate can reach 70%. Ramos *et al.* (2022) used wet chemical precipitation to synthesize HAP, copper-doped HAP with different concentrations and Cu*x*–HAP ($x = 1$, 2, and 4 mol%) nanomaterials. Complex analysis and spectroscopic techniques were employed to confirm their physicochemical properties and morphological characteristics. The results indicate that Cu*x*–HAP nanomaterials exhibit stronger biocompatibility and mechanical stability.

Based on the above discussion, in this paper, we aim to synthesize an efficient catalyst for the degradation of phenol in water by loading Cu^{2+} onto HAP. The aim is to overcome the shortcomings of the traditional Fenton oxidation reaction such as narrow pH range and the strong reliance on operational conditions.

2. MATERIAL AND METHODS

2.1. Characterization

The scanning electron microscopic (SEM) analysis was conducted using the Zeiss Gemini 300 instrument. X-ray diffraction (XRD) measurements were performed using the Bruker D8 Advance X-ray diffractometer with Cu-Kα radiation and a diffraction angle range of 10°–80° (voltage = 40 kV, current = 40 mA). Fourier-transform infrared (FTIR) spectroscopy was carried out using the Thermo Scientific Nicolet 6700 infrared spectrometer, covering a spectral range of 4,000–500 cm^{-1}. The nitrogen adsorption–desorption isotherm characterization (Brunauer–Emmett–Teller, BET) was determined using a 77 K ASAP 2020 PLUS surface area and a porosity analyzer.

2.2. Materials and reagents

The chemicals used in the experiment were of analytical purity. Hydrochloric acid, sodium hydroxide, HAP, copper sulfate pentahydrate, acetic acid, sodium acetate, sodium tetraborate pentahydrate, ethanol, and phenol were purchased from Sinopharm Chemical Reagent Co., Ltd. Boric acid was purchased from Thailand Chemical Reagent Factory, which is located in Dongli District, Tianjin. Bicyclohexanone oxalyl diamine was purchased from Ron Reagent. Hydrogen peroxide was purchased from Tianjin Tianli Chemical Reagent Co., Ltd. The pH adjustment to the desired level was accomplished using a 0.2 mol/L acetic acid–sodium acetate buffer solution prepared by adjusting with a 0.3 mol/L acetic acid solution. Similarly, the pH of the sodium tetraborate–boric acid buffer solution (0.05 mol/L, pH = 9.19) was adjusted using a certain amount of boric acid to achieve a pH value of 8.5. The copper ion standard stock solution (1,000 mg/L), bicyclohexanone oxalyldihydrazone standard solution (500 mg/L), phenol standard solution (50 mg/L), and phenol aqueous solution (50 mg/L) were prepared by appropriate agents and pure water.

2.3. Preparation of Cu–HAP catalyst

A copper ion solution of precise concentration was formulated through dilution with distilled water. The relative Cu^{2+} dosage to HAP was maintained at 100 mg/g. The prepared solutions were subjected to controlled agitation in a thermostatic oscillator within the temperature range of 25–45 °C for a duration of 6 h. The stirring speed was set at a constant of 200 rpm. The resulting catalysts were denoted as Cu–HAP-25 to Cu–HAP-45. Subsequently, the prepared Cu–HAP catalyst was introduced at a relative dosage of 1.0 g/L into a 50 mL aqueous solution containing phenol with a concentration of 50 mg/L. Additionally, a 30% hydrogen peroxide solution, specifically 19.54 mmol/L (equivalent to 0.15 mL), was incorporated. The mixture was agitated under thermostatic conditions at a constant temperature of 25 °C and a stirring speed of 200 rpm. Following a reaction duration of 1 h, the solution was subjected to centrifugation, and the supernatant was separated by filtration through a 0.45 μm filter. All reactions were meticulously performed under light-shielded conditions, with each condition replicated in three parallel experiments. Based on the acquired results, the optimal temperature for the preparation process was determined. At this optimized temperature, the relative dosage of Cu^{2+} to HAP was systematically regulated at 100, 200, 300, 400, and 500 mg/g while keeping the remaining parameters constant. Consequently, the resulting catalysts were denoted as Cu–HAP-100 to Cu–HAP-500. Furthermore, the Cu–HAP preparation process was conducted under unchanging conditions, except for the pH values, which were set to 3, 4, 5, 6, 7, 8, and 9. The catalysts obtained from these experimental variations were designated as Cu–HAP-3–Cu–HAP-9.

2.4. Removal experiment of phenol

By means of influence factor experiments, precise control was exercised over the relative dosage of Cu–HAP (ranging from 1.0 to 5.0 g/L), the dosage of 30% hydrogen peroxide solution (varying from 3.91 to 191.96 mmol/L or 0.02 to 1 mL), the initial concentration of phenol (ranging from 10 to 50 mg/L), the initial pH (ranging from 3 to 7), and the reaction temperature (set at 25, 30, 35, 40, and 45 °C). These experiments were conducted within a thermostatic oscillator, allowing for agitation for a duration of 1 h at a constant stirring speed of 200 rpm. Upon the conclusion of the reaction, the samples underwent filtration utilizing a 0.45 μm filter, thereby facilitating the determination of the residual phenol concentration. It is noteworthy that all reactions were diligently carried out under conditions that obviated exposure to light while ensuring the meticulous execution of three parallel experiments.

2.5. Determination of the loading capacity and the loading rate of Cu^{2+}

In this study, the concentration of copper ions was determined using bicyclohexanone oxalyl diamine. The content of copper ions in the supernatant and washing solution was measured, and the loading amount (Ld, mg/g) and the loading rate (Lr, %) of copper ions were obtained. The specific formulas are as follows:

$$\mathrm{Ld} = \frac{m_i - m_f}{M}$$

$$\mathrm{Lr} = \frac{m_i - m_f}{m_i} * 100\%$$

m_i is the initial copper ion content, mg; m_f is the Cu^{2+} content in the supernatant and washing solution, mg; and M is the initial catalyst mass, g.

2.6. Determinations of the copper ion leaching rate and the catalyst loss rate

The calculation formulas of the copper ion leaching rate (Lr, %) and the catalyst loss rate (Ls, %) are as follows:

$$Lr = \frac{m_s + m_d}{m_i} * 100\%$$

$$Ls = \frac{M - M_f}{M} * 100\%$$

m_s is the copper ion content in the supernatant, mg; m_d is the copper ion content in the washing solution, mg; M is the initial catalyst mass, mg; M_f is the final catalyst mass, mg.

2.7. Determination of phenol content

A standard solution of phenol with a concentration of 50 mg/L was prepared as a stock solution. Volumes of 2.5, 5, 7.5, 10, 12.5, 15, 17.5, 20, and 25 mL were measured from the stock solution and diluted to 25 mL in volumetric flasks. The concentration of phenol in these solutions was determined using the high-performance liquid chromatography (HPLC) method. The HPLC system utilized a Thermo SCIENTIFIC C18 reversed-phase column (250 mm × 4.6, 5 μm), with a flow rate of 1.0 mL/min. The mobile phase consisted of a mixture of methanol and water in a volume ratio of 75:25. The detection wavelength was set at 270 nm, and the column temperature was maintained at 35 °C. A sample injection volume of 20 μL was used. The linear regression equation was obtained from the linear fit: $y = 0.35186x + 0.3127$, $R^2 = 0.9983$.

The phenol content in the solution to be measured is determined by the above method. The formula of the phenol removal rate (Re, %) is as follows:

$$\mathrm{Re} = \frac{c_{e0} - c_{et}}{c_{e0}} * 100\%$$

c_{e0} is the initial phenol concentration, mg /L; c_{et} is the t time phenol concentration, mg/L.

2.8. Determination of phenol degradation intermediates

The identification of intermediate products resulting from the degradation of phenol in water was carried out using gas chromatography–mass spectrometry (GC/MS) analysis. The purging step was performed under specific conditions: a purging time of 11.0 min and purging gas composed of nitrogen (N_2) (>99.999%) at a flow rate of 40.0 mL/min. The resolution temperature was set at 185 °C for a duration of 40 min, followed by a baking temperature of 200 °C for 20 min. Chromatographic conditions included split injection with a split ratio of 20:1. The injection port temperature was set at 185 °C. High-purity helium (99.999%) was used as the carrier gas, with a constant flow rate of 1.0 mL/min. The temperature program for the chromatographic column involved a gradual increase from 60 to 100 °C over 20 min, followed by a rapid temperature rise to 220 °C at a rate of 30 °C/min for 5 min. For mass spectrometry analysis, a solvent delay time of 4.0 min was implemented. The voltage was set at 1,049 V, and the ion source temperature (electron impact ionization, EI) was maintained at 230 °C. The temperature of the fourth stage rod was set to 150 °C. The monitoring ions selected were at mass-to-charge ratios (M/Z) of 94, 66, 55, and 39, with a quantitative ion at 94.3.

3. RESULTS AND DISCUSSION

3.1. Characterization

Figure 1 shows the characterization results using SEM, BET, XRD, and FTIR. Figure 1(a) and 1(b) depicts the microstructure before and after Cu^{2+} loading on HAP observed through SEM. It can be observed that HAP itself has a porous structure with a large specific surface area. After Cu^{2+} loading, the particle size decreases, and more pore structures are formed, indicating that the introduction of Cu^{2+} makes the sample more uniform with reduced particle size.

Figure 1(c) shows the N_2 adsorption–desorption isotherm of Cu–HAP. The common adsorption isotherms are classified into six types. Type I isotherm curves toward the P/P_0 axis and the subsequent images are nearly horizontal. Type II isotherms have inflection point B at low P/P_0, which is the first steep break of the isotherm. Type III isotherms are internally convex downward throughout the pressure range and the curve has no inflection point. Type IV isotherm is convex upward in the curve at low P/P_0, and at high P/P_0, the adsorbate undergoes capillary condensation and the isotherm

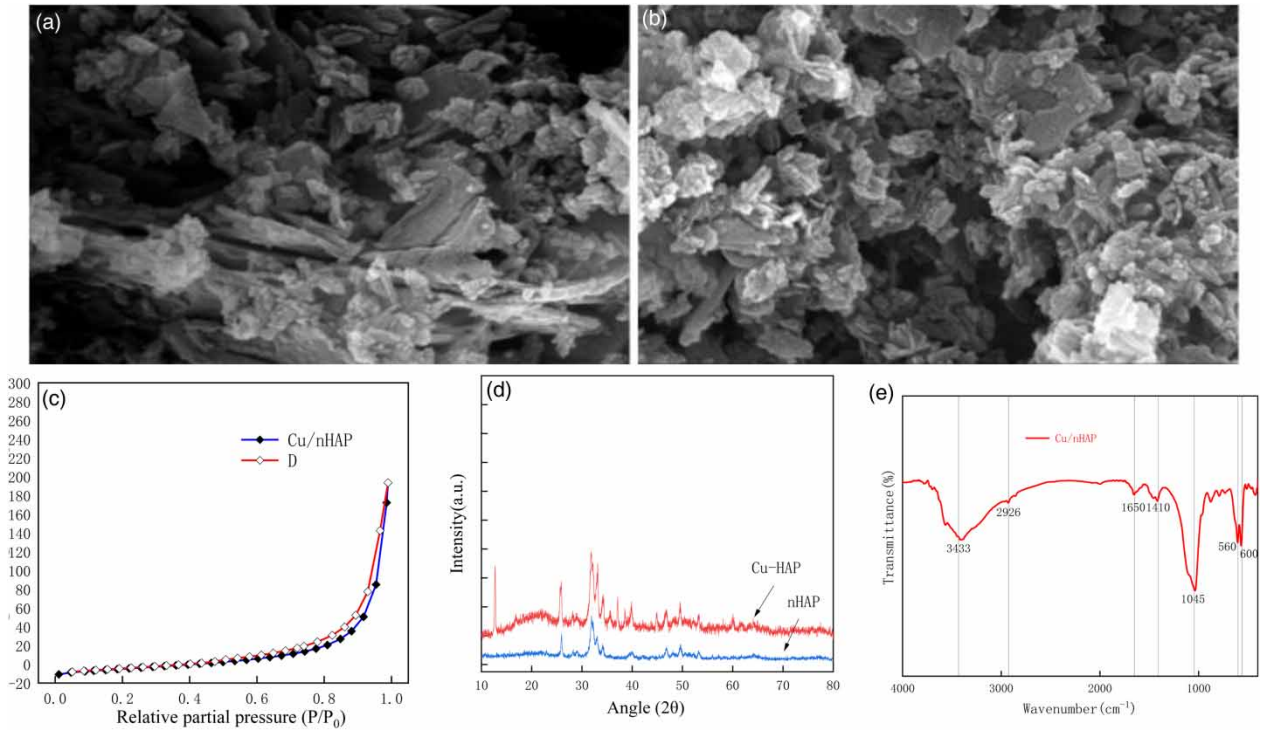

Figure 1 | SEM (a and b) of HAP before and after loading Cu^{2+}, BET (c) of Cu–HAP, XRD (d) of HAP, and Cu–HAP and FTIR (e) of Cu–HAP.

rises rapidly, and a hysteresis phenomenon can be observed when the relative pressure is close to 1, presenting a hysteresis loop. Type V isotherm is very similar to type III at lower P/P_0, but there is an inflection point at higher relative pressure. Type VI isotherm presents a step-like reversible adsorption process. The adsorption isotherm of Cu–HAP is known to be type IV from the figure below because the adsorption and desorption curves of the isotherm are clearly inconsistent with the presence of hysteresis. This indicates that Cu–HAP has a mesoporous structure, which is consistent with the observation of SEM images.

Figure 1(d) presents the XRD spectra of HAP before and after Cu^{2+} loading. The characteristic peaks of HAP can be identified in the XRD spectrum of the Cu–HAP catalyst, indicating that the introduction of Cu^{2+} does not alter the crystal structure of HAP. Thus, the catalyst retains the stability of HAP.

Figure 1(e) shows the FTIR spectrum of Cu–HAP. The peak at 1,045 cm^{-1} corresponds to the stretching and bending vibrations of P–O in PO_3^{2-} (Gonzalez-McQuire *et al.* 2004). Peaks near 1,650 and 3,433 cm^{-1} correspond to the bending vibrations of –OH in physically adsorbed water molecules (Jamil *et al.* 2020). The peak at 2,926 cm^{-1} corresponds to the stretching of C–H bonds (Gonzalez-McQuire *et al.* 2004). The peak at 3,433 cm^{-1} is attributed to the hydroxyl groups in HAP and physically absorbed water molecules (Yelten-Yilmaz & Yilmaz 2018). These characteristic peaks confirm the presence of relevant functional groups in HAP, consistent with the XRD characterization results. Compared to HAP, the peak intensity of Cu–HAP slightly increases, indicating an increase in crystallinity after copper doping. However, Cu–HAP still exhibits the structural properties of HAP. These results indicate that the six-fold symmetry of the crystal is not significantly altered when calcium ions in HAP are replaced by equivalent copper ions. Compared with the study by Krishna & Siddhartha (2021) on Cu/HAP/$ZnFe_2O_4$ nanocomposites, the characteristic peak at 1,045 cm^{-1} slightly deviates. This slight deviation is attributed to the strong interaction between the copper electrode and the carrier material, confirming the presence of a chemical bond between the copper element and the carrier material.

3.2. Factors affecting the preparation of Cu–HAP

3.2.1. Factors affecting Cu^{2+} loading capacity and the loading rate

The mechanism of HAP loading of copper ions is that Ca^{2+} on the top of HAP undergoes ion exchange with Cu^{2+}. Krishna & Siddhartha (2021) proposed that there are two sites for the ion exchange of HAP with cations (Kawasaki

et al. 1990). One is that part of Ca^{2+} on the c-surface is connected to six negatively charged O atoms (CaI), and the other part of Ca^{2+} on the c-surface is connected to three negatively charged O atoms (CaII). Ca^{2+} at both sites can undergo ion exchange with metal ions. It was shown that metal ions with smaller ionic radii than Ca^{2+} are preferentially exchanged with Ca^{2+}(I) and metal ions with larger ionic radii than Ca^{2+} are preferentially exchanged with Ca^{2+}(II). Since Cu^{2+} radius of 0.073 nm is smaller than Ca^{2+} radius of 0.099 nm, it is easier to occupy the position of CaI. However, Baravelli *et al.* (1984) speculated that Cu^{2+} is more likely to take the place of CaII by structural modeling and extended X-ray absorption fine structure spectroscopy (EXAFS). The substitution position of copper ions in the Cu–HAP in this study needs to be further investigated, but it suggests that the number of cation exchange sites in HAP is limited. Therefore, the copper ion loading rate and loading amount will not increase after the exchange of copper and calcium ions reaches saturation.

The following figure explores the effects of temperature, relative Cu/HAP dosage, and pH on copper ion loading and loading rate. As shown in Figure 2(a), both copper ion loading and loading rate of Cu–HAP increased with the increase of preparation temperature. A cliff-like increase occurs when the temperature is greater than 40 °C, and the copper loading reaches 100.34 mg/g and the copper loading rate reaches 98.40%, which almost loads all the injected copper. The temperature continued to increase the copper loading amount and the copper loading rate did not change much. The reason for this result is that the temperature increases, the thermal movement of ions accelerated, and the opportunity for copper ions to contact HAP increased, so the loading amount and the loading rate will rise. From the mechanism section above, it is also known that the number of sites where HAP can undergo ion exchange is limited. Therefore, when the temperature continues to rise, HAP cannot provide more ion exchange sites, so the loading amount and the loading rate no longer rise.

As shown in Figure 2(b), the copper ion loading of Cu–HAP increased with the increase in the relative amount of copper up to 96.01 mg/g. However, the copper ion loading decreased with the increase of the relative amount of copper, and the loading decreased to 35.22% when the relative amount of copper was 100 mg/g. This also confirms that the ion exchange sites of HAP are limited.

As shown in Figure 2(c), the copper loading image of Cu–HAP showed an increasing and then decreasing trend with respect to pH. The highest value of 106.06 mg/g was reached at pH 5. But the copper loading rate continued to increase with pH, achieving a cliff-like increase at pH greater than 5 and a maximum copper loading rate of 98.78% at pH 9. This is attributed to the dissolution of HAP at low pH and the precipitation of copper ions at high pH.

3.2.2. Factors affecting phenol removal by preparation conditions

Figure 3 investigates the impact of various preparation temperatures, different Cu/HAP relative dosages, and pH values on the phenol removal rate. As depicted in Figure 4(a), the phenol removal rate corresponding to Cu–HAP decreases as the preparation temperature increases. At a preparation temperature of 25 °C, the phenol removal rate is 64.94%. However, the lowest phenol removal rate of 28.98% is observed at a preparation temperature of 45 °C.

In Figure 3(b), the phenol removal rate corresponding to Cu–HAP prepared with different copper-relative dosages increases with dosage. The maximum phenol removal rate of 83.35% is achieved at a copper-relative dosage of 500 mg/g, while the minimum phenol removal rate of 62.46% is observed at a copper-relative dosage of 100 mg/g. It is noteworthy that, based

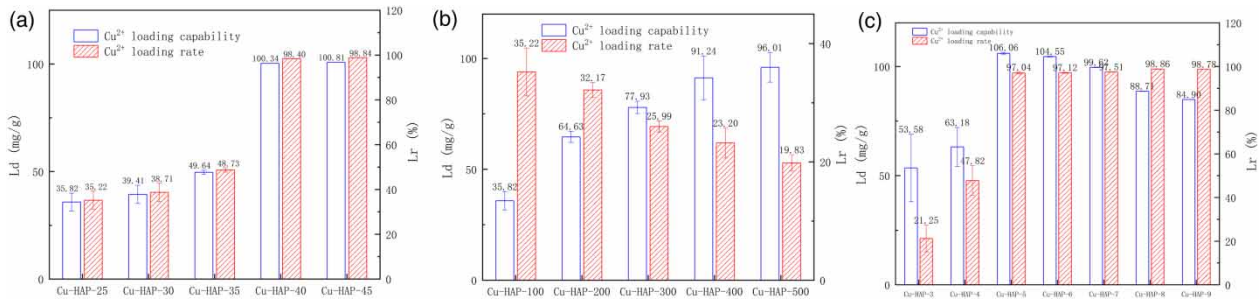

Figure 2 | The effect of temperature (a), Cu/HAP relative dosage (b), and pH (c) on the copper ion loading rate and loading capacity.

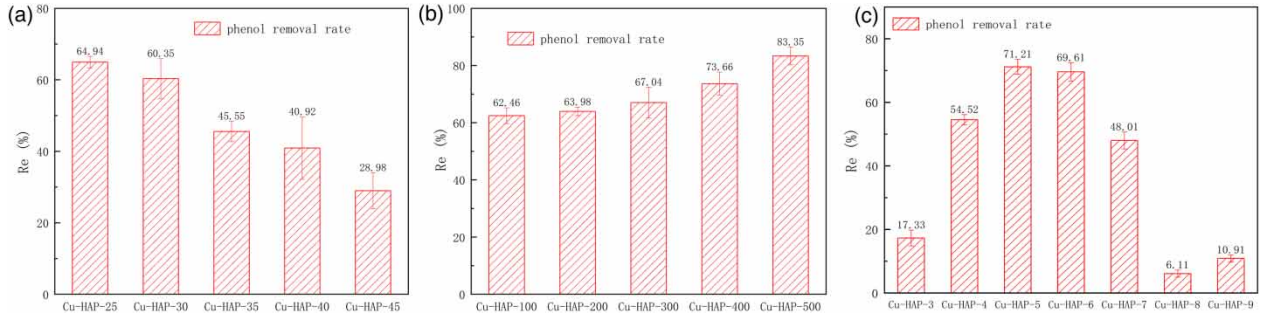

Figure 3 | Effect of different preparation temperature (a), relative dosage of Cu/HAP (b), and pH (c) on the phenol removal rate.

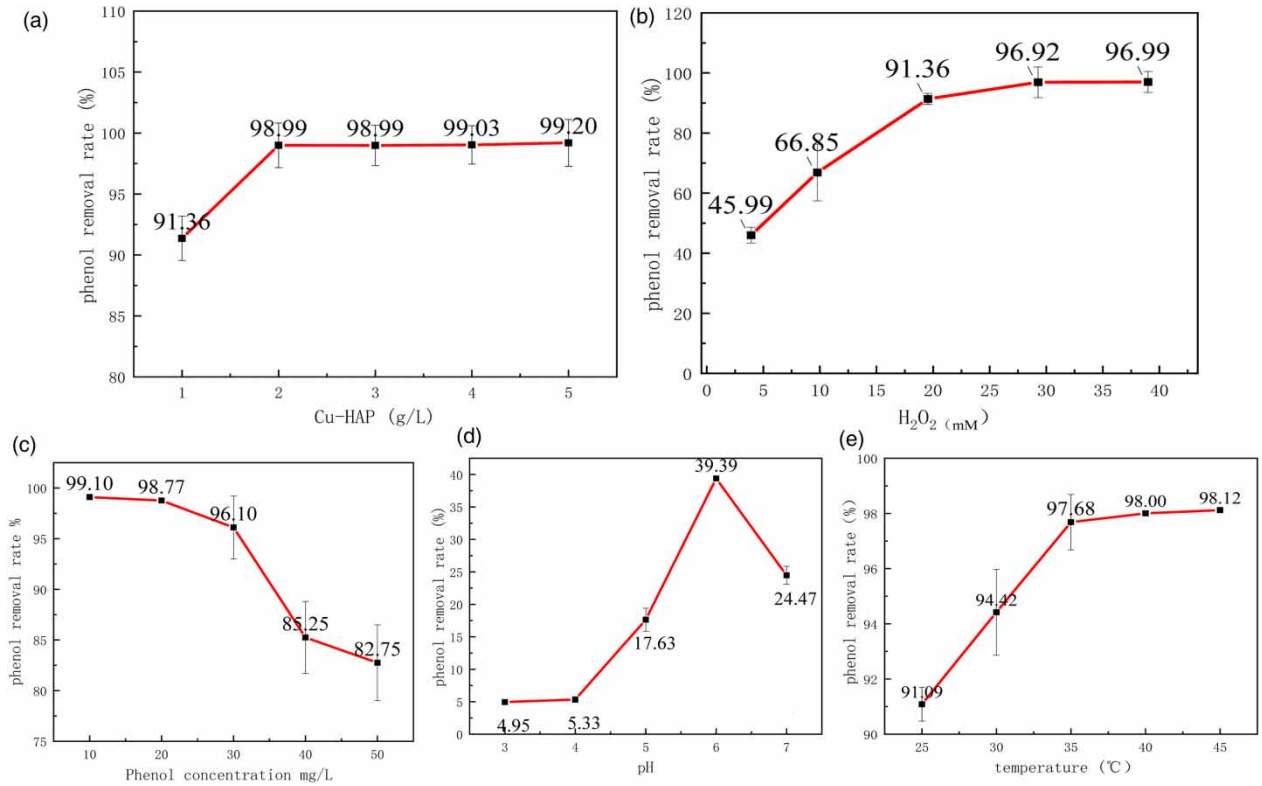

Figure 4 | Effects of catalyst dosage (a), oxidant dosage (b), phenol concentration (c), pH (d), and reaction temperature (e) on the phenol removal rate.

on the relationship between the copper ion loading rate and the preparation temperature and relative dosage of HAP, the highest copper ion loading rate is observed at a preparation temperature of 45 °C and a relative dosage of 500 mg/g. However, this condition corresponds to the lowest phenol removal rate. This phenomenon can be attributed to the nearly complete occupation of surface sites on HAP by Cu^{2+} due to monolayer adsorption. Consequently, phenol molecules lack available binding sites, resulting in a reduction in the phenol removal rate.

Figure 3(c) illustrates that the phenol removal rate and catalytic activity of Cu–HAP prepared at different pH values initially increase and then decrease. The highest phenol removal rate of 71.21% is achieved at pH 5. Notably, a sharp decline in phenol removal rate and catalytic activity occurs when pH exceeds 8. This observation can be primarily attributed to the requirement for acidic conditions in the catalytic decomposition reaction of hydrogen peroxide.

3.3. Factors affecting the phenol removal rate

The impact of catalyst dosage, oxidant dosage, initial phenol concentration, pH, and reaction temperature on phenol removal efficiency is discussed as follows. As illustrated in Figure 4(a), the phenol removal efficiency initially increases and then reaches a plateau as the catalyst dosage increases. The inflection point, where the phenol removal rate reaches 98.99%, is observed at a dosage of 2 g/L. This behavior can be attributed to the provision of additional active sites for H_2O_2 when the catalyst dosage is low. However, beyond a certain dosage, the surplus content of the catalyst leads to negligible improvement in the phenol removal rate. Therefore, the optimal catalyst dosage is determined to be 2 g/L.

In Figure 4(b), the phenol removal rate gradually increases with an increase in oxidant dosage. The inflection point, where the removal rate is 96.92%, is achieved when the oxidant dosage reaches 30 mM. Further increasing the oxidant dosage has a minimal effect on the phenol removal rate. This is because an excessive amount of H_2O_2 may react with hydroxyl radicals, failing to further enhance the removal rate. Thus, the optimal oxidant dosage is determined to be 30 mM.

Figure 4(c) demonstrates that the phenol removal rate maintains a high level when the initial phenol concentration is low (10–20 mg/L), remaining at around 98%. As the initial concentration increases, the phenol content gradually decreases. At an initial concentration of 50 mg/L, the removal rate reaches a minimum of 82.75%. This outcome arises from the limited increase in hydroxyl radicals released by H_2O_2 as the phenol concentration rises, hindering the ability to contact more phenol and enhance the removal rate.

In Figure 4(d), the phenol removal rate initially increases and then decreases with an increase in pH. The maximum removal rate of phenol, reaching 39.39%, is achieved at a pH value of 6. Subsequently, the removal rate decreases as pH increases. This phenomenon may be attributed to the complete precipitation of copper ions at pH 6.4, which is unfavorable for Fenton-like reactions.

Figure 4(e) reveals that the phenol removal rate initially increases and then stabilizes as the reaction temperature rises. The inflection point, where the phenol removal rate is 97.68%, occurs at 35 °C. This behavior can be explained by the fact that while an elevated reaction temperature promotes the reaction between hydroxyl radicals and phenol due to enhanced molecular thermal movement, it also accelerates the decomposition of H_2O_2 in a (similar) Fenton system. Consequently, the generation of oxygen and water hinders the production of hydroxyl radicals, resulting in a decrease in the phenol removal rate with increasing temperature.

3.4. Reusability of Cu–HAP

Cu–HAP was synthesized using the optimized parameters, and the phenol removal rate was evaluated under the optimal degradation conditions. Following the experiment, Cu–HAP was subjected to recycling procedures, including washing,

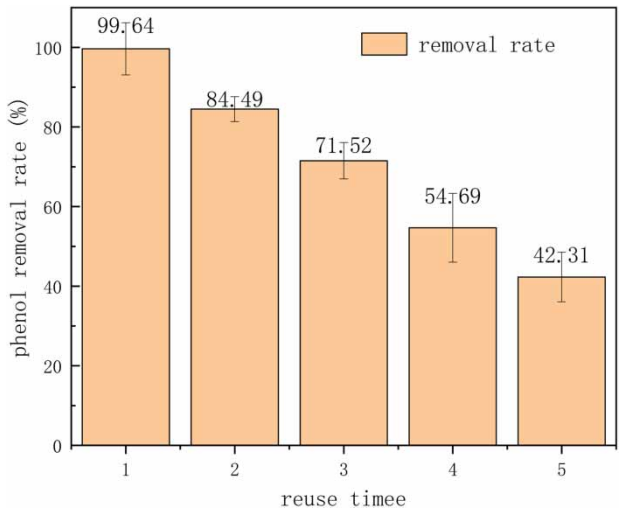

Figure 5 | Reusability of Cu–HAP (40 °C, 20 mg/L phenol, dosage of Cu–HAP 2 g/L, H_2O_2 30 mM, pH = 6, 1 h).

filtration, and drying, to facilitate its reusability. It is noteworthy that Cu–HAP still showed some catalytic activity after five cycles of reuse, with a phenol removal rate of 42.31% (Figure 5). This result indicates that Cu–HAP possesses passable reusability, making it suitable for various applications.

3.5. Phenol degradation mechanism

High-performance liquid chromatography (HPLC) allows for the quantitative analysis of residual organic pollutants but does not provide insights into the intermediate products produced during pollutant degradation. To elucidate the degradation process of organic pollutants and determine the appropriate treatment method, gas chromatography–mass spectrometry (GC/MS) is employed. By analyzing the pollutant structure, degradation characteristics, and examining the detected intermediate products, it becomes possible to predict the pollutant degradation process, thereby establishing a theoretical foundation for enhancing degradation efficiency. Figure 6 presents the GC/MS results showcase the intermediate products generated during phenol degradation. Notably, three significant intermediates are observed within the degradation system, namely p-benzoquinone, p-phenol, and maleic acid. Table 1 shows the chemical structures of the relevant intermediates and the GC/MS peaks.

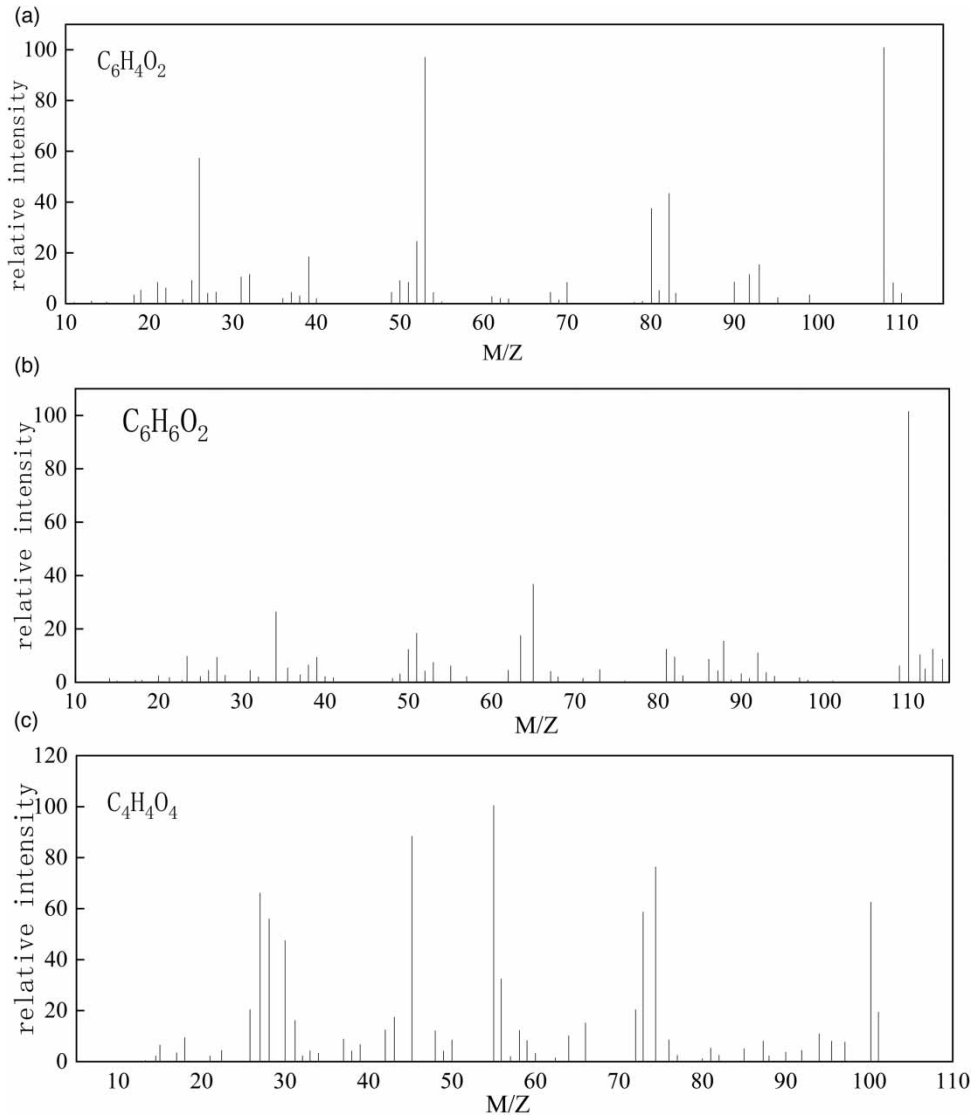

Figure 6 | Mass spectrum of phenol degradation intermediate.

Table 1 | Structure of intermediates

Intermediate	$C_6H_4O_2$	$C_6H_6O_2$	$C_4H_4O_4$
Structural formula	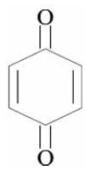	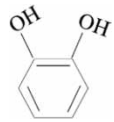	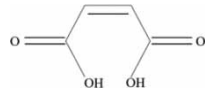
Mass nucleus ratio	53.0	110.1	55.0

Based on the mechanism of the Fenton catalytic system, we hypothesize that in the Cu–HAP, the catalyzed oxidation of phenol radicals by hydrogen peroxide proceeds as follows (Baravelli *et al.* 1984; Edward *et al.* 2010; Enric & Sergi 2020):

$$Cu^{2+} + H_2O_2 \rightarrow Cu^{+} + HO_2^{\bullet} + H^{+}$$

$$Cu^{+} + H^{+} + H_2O_2 \rightarrow Cu^{2+} + H_2O + {}^{\bullet}OH$$

$$RH + {}^{\bullet}OH \rightarrow R^{\bullet} + H_2O$$

$$R^{\bullet} + H_2O_2 \rightarrow ROH + {}^{\bullet}OH$$

$${}^{\bullet}OH + H_2O_2 \rightarrow H_2O + HO_2^{\bullet}$$

$$HO_2^{\bullet} \rightarrow O_2 + H^{+}$$

$$Cu^{2+} + R^{\bullet} \rightarrow Cu^{+} + R^{+}$$

$$O_2 + R^{\bullet} \rightarrow ROO^{+} \ldots \rightarrow CO_2 + H_2O$$

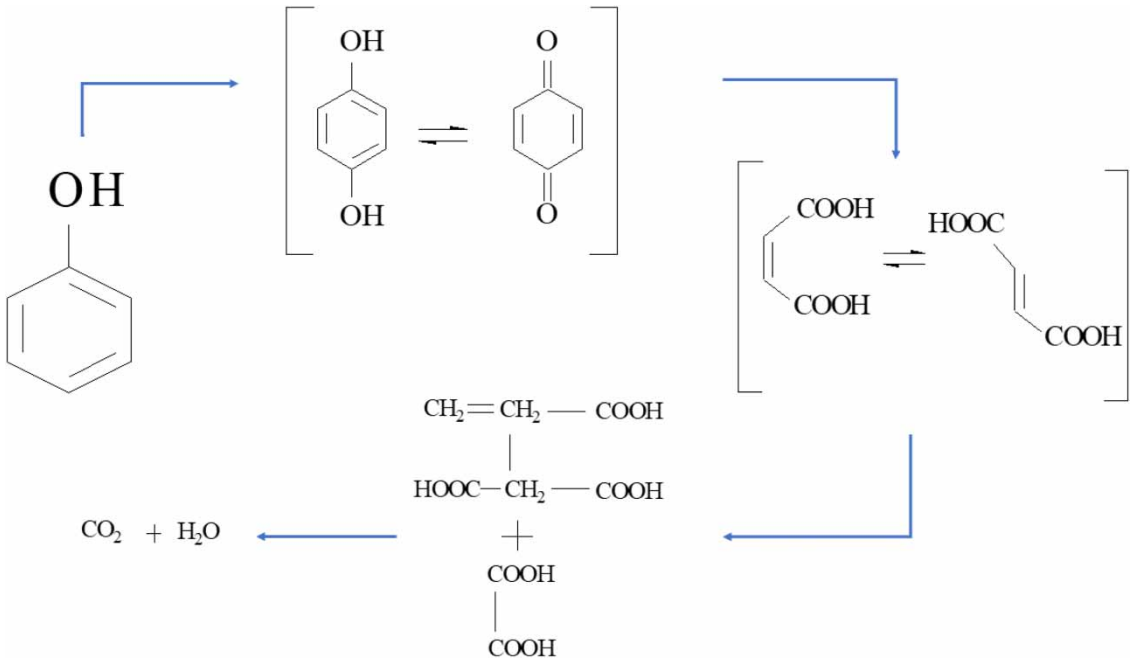

Figure 7 | Possible phenol degradation process.

It can be inferred that in the reaction system of Cu–HAP catalyzed H_2O_2 oxidation of phenol initially, Cu^+ is oxidized by H_2O_2 to Cu^{2+}, and H_2O_2 is also reduced to $HO^{\cdot}$ in the process, which firstly attacks the para-site of phenol and mainly produces hydroquinone. This is an important product of phenol hydroxylation. During the subsequent degradation phase, the electron-deficient benzoquinone is attacked by hydroxyl radicals, resulting in a molecular ring opening. This ring-opening process leads to the degradation of benzoquinone to a variety of carboxylic acids, which may include fumaric, maleic, oxalic and acetic acids, and ultimately to complete catalytic oxidation. Based on the literature (Enric & Sergi 2020), it is hypothesized that catechol opens the ring to form hexadienedioic acid. Hexadienedioic acid is further oxidized to form maleic and trans-butylene diacid. Of these, maleic acid is the main product of ring cleavage. However, it is worth noting that these intermediates are eventually fully oxidized to water (H_2O) and carbon dioxide (CO_2). In conjunction with the HPLC results, Figure 7 demonstrates a possible process for the degradation of phenol by H_2O_2 catalyzed by Cu–HAP.

4. CONCLUSION

Within the context of this study, a novel composite material, denoted as Cu–HAP, was synthesized and employed as a catalyst for phenol removal reactions. Remarkably, under optimized conditions, the phenol removal rate achieved 98.12%. After undergoing five cycles of repeated use, the Cu–HAP catalyst maintained a passable phenol removal rate of 42.31%. These results indicate a certain degree of industrial application potential for this material.

ACKNOWLEDGEMENTS

This work was supported by the Science and Technology Innovation Team Project of Hubei Provincial Department of Education (Grant No. T2020002), Wuhan Science and Technology Planning Project (Grant No. 2020020601012274), National Natural Science Foundation of China (Grant No. 41571306), and Hubei Technological Innovation Special Fund (Grant No. 2020ZYYD019). The authors would like to thank Jiang Lang from Shiyanjia Lab (www.shiyanjia.com) for the characterization support.

DATA AVAILABILITY STATEMENT

All relevant data are included in the paper or its Supplementary Information.

CONFLICT OF INTEREST

The authors declare there is no conflict.

REFERENCES

Baravelli, S., Bigi, A., Ripamoti, A., Roveri, N. & Foresti, E. 1984 Thermal behavior of bone and synthetic hydroxyapatites submitted to magnesium interaction in aqueous medium. *Journal of Inorganic Biochemistry* **20** (1), 1–12.

Edward, A. K., Anton, L. M., Yulia, S. K., Vitaliy, A. S., Sergey, V. K., Viktoriya, V. P., Marta, Y. T., Elena, L., Jeffrey, A. S. & Scott, L. C. 2010 Copper nanoparticles as active catalysts in hydroxylation of phenol by hydrogen peroxide. *Applied Catalysis A: General* **385** (1–2), 62–72.

Enric, B. & Sergi, G. 2020 Benchmarking recent advances and innovative technology approaches of Fenton, photo-Fenton, electro-Fenton, and related processes: a review on the relevance of phenol as model molecule. *Separation and Purification Technology* **237**, 116337.

Gonzalez-McQuire, R., Chane-Ching, J., Vignaud, E., Lebugle, A. & Mann, S. 2004 Synthesis and characterization of amino acid-functionalized hydroxyapatite nanorods. *Journal of Materials Chemistry* **14**, 2277–2281.

Imane, H., Khalid, A., Savaş, K., Taner, D., Naaila, O., Laila, M. & Faissal, A. 2023 Green synthesis of reduced graphene oxide and their use on column adsorption of phenol from olive mill wastewater. *Process Safety and Environmental Protection* **170**, 1079–1091.

Jamil, M., Elouahli, A., Abida, F., Khallok, H., Gourri, E., Kheribech, A. & Hatim, Z. 2020 Development of triphasic hydroxyapatite/(α and β)-tricalcium phosphate based composites by sintering powder of calcium-apatite in the presence of montmorillonite. *Journal of Inorganic and Organometallic Polymers and Materials* **30**, 2489–2498.

Jian, L. W. & Le, J. X. 2012 Advanced oxidation processes for wastewater treatment: formation of hydroxyl radical and application. *Critical Reviews in Environmental Science and Technology* **42** (3), 251–325.

Jingxin, S., Jin, W., Ning, W., Jie, Q., Shuai, L., Lang, X., Chenxu, W. & Hongjun, H. 2022 Treatment of phenols and NH_3–N with activated carbon and polyurethane carrier in biological enrichment reactor. *Journal of Cleaner Production* **369**, 133251.

Kawasaki, T., Niikura, M. & Kobayashi, Y. 1990 Fundamental study of hydroxyapatite high-performance liquid chromatography: III. Direct experimental confirmation of the existence of two types of absorbing surface on the hydroxyapatite crystal. *Journal of Chromatography A* **515** (31), 125–148.

Krishna, C. D. & Siddhartha, S. D. 2021 Fast catalytic reduction of p-nitrophenol by Cu/HAP/$ZnFe_2O_4$ nanocomposite. *Materials Science and Engineering: B* **263**, 114841.

Kuan, Z. H. & Huichun, Z. 2019 Direct electron-transfer-based peroxymonosulfate activation by iron-doped manganese oxide (δ-MnO_2) and the development of Galvanic Oxidation Processes (GOPs). *Environmental Science & Technology* **53** (21), 12610–12620.

Kuan, H. & Huichun, Z. 2022 A comprehensive kinetic model for phenol oxidation in seven advanced oxidation processes and considering the effects of halides and carbonate. *Water Research X* **14**, 100129.

Lili, Z., Dan, X., Chun, H. & Yilun, S. 2017 Framework Cu-doped $AlPO_4$ as an effective Fenton-like catalyst for bisphenol A degradation. *Applied Catalysis B: Environmental* **207**, 9–16.

Liu, Y., Cheng, M., Liu, Z., Zeng, G., Zhong, H., Chen, M., Zhou, C., Xiong, W., Shao, B. & Song, B. 2019 Heterogeneous Fenton-like catalyst for treatment of rhamnolipid-solubilized hexadecane wastewater. *Chemosphere* **236**, 124387.

Ludmila, C. N., Jeanette, B. S., Carlos, M. S. V., Lucila, T. H., Kely, V. S., Kelly, G. M. & Brian, J. Y. 2020 Phytotoxicity indexes and removal of color, COD, phenols and ISA from pulp and paper mill wastewater post-treated by UV/H_2O_2 and photo-Fenton. *Ecotoxicology and Environmental Safety* **202**, 110939.

Othmani, M., Bachoua, H., Ghandour, Y., Aissa, A. & Debbabi, M. 2018 Synthesis, characterization and catalytic properties of copper-substituted hydroxyapatite nanocrystals. *Materials Research Bulletin* **97**, 560–566.

Panigrahy, N., Barik, M., Sahoo, R. K. & Sahoo, N. K. 2020 Metabolic profile analysis and kinetics of p-cresol biodegradation by an indigenous *Pseudomonas citronellolis* NS1 isolated from coke oven wastewater. *International Biodeterioration & Biodegradation* **147**, 104837.

Qian, K., Yunge, Z., Xilin, W., Xiaomei, S., Yuyang, W., Hongjun, L., Rongwu, M., Yu, Z., Muhammad, Z. H., Chongjun, C. & Jianrong, C. 2018 Sustainable biodegradation of phenol by immobilized Bacillus sp. SAS19 with porous carbonaceous gels as carriers. *Journal of Environmental Management* **222**, 185–189.

Ramos, M. D. N., Velloso, C. S., Da Silva, A. H. M., Magalhaes, F. & Aguiar, A. 2021 A review on the treatment of textile industry effluents through Fenton processes. *Process Safety and Environmental Protection* **155**, 366–386.

Ramos, P. S., Choi, J., Mondal, S., Vo, T. M. T., Pharm, V. H., Lee, H., Nam, S. Y., Kim, C. & Oh, J. 2022 The impact of Cu(II) ions doping in nanostructured hydroxyapatite powder: a finite element modelling study for physico-mechanical and biological property evaluation. *Advanced Power Technology* **33** (2), 103405.

Santiago, E., Jaime, G., Sandra, C., Esther, P. & Miguel, R. 2002 Comparison of different advanced oxidation processes for phenol degradation. *Water Research* **36** (4), 1034–1042.

Weihua, Q., Mingye, R., Yuwei, L. & Shaoxia, Y. 2022 High effective degradation of phenol with Cu/Bi-Ce/Al_2O_3 heterogeneous Fenton-like catalyst in a two-stage fixed-bed reactor. *Separation and Purification Technology* **299**, 121733.

Xiaoguang, D., Hongqi, S., Zongping, S. & Shaobin, W. 2018 Nonradical reactions in environmental remediation processes: uncertainty and challenges. *Applied Catalysis B: Environmental* **224**, 973–982.

Yelten-Yilmaz, A. & Yilmaz, S. 2018 Wet chemical precipitation synthesis of hydroxyapatite (HA) powders. *Ceramics International* **44** (8), 9703–9710.

Yu, L. & Hefa, C. 2022 Autocatalytic effect of in situ formed (hydro)quinone intermediates in Fenton and photo-Fenton degradation of non-phenolic aromatic pollutants and chemical kinetic modeling. *Chemical Engineering Journal* **449**, 137812.

Zhaobo, W., Dajun, R., Shanshan, S., Shuqin, Z., Xiaoqing, Z. & Wangsheng, C. 2022 Novel synthesis of Cu-HAP/SiO_2@carbon nanocomposites as heterogeneous catalysts for Fenton-like oxidation of 2,4-DCP. *Advanced Powder Technology* **33** (3), 103509.

Zhuangzhuang, Z., Haiqian, Z., Zhonghua, W., Zhipei, H., Qingshu, W., Me, E., Shiwei, L., Jiaxin, Y., Hongguang, L. & Chuanyan, W. 2023 Strategies for promoting the degradation of phenol by electro-Fenton: simultaneously promoting the generation and utilization of H_2O_2. *Environmental Research* **236**, 116794.

First received 15 July 2023; accepted in revised form 29 August 2023. Available online 13 September 2023